Exact solutions for static analysis of laminated, box and sandwich beams by refined layer-wise theory

Exact solutions for static analysis of laminated, box and sandwich beams by refined layer-wise theory

A. Pagani[a*], Y. Yan[ab†], E. Carrera[a‡]

[a] *Mul^2, Department of Mechanical and Aerospace Engineering, Politecnico di Torino*
Corso Duca degli Abruzzi 24, 10129 Torino, Italy.

[b] *College of Mechanics and Materials, Hohai University*
210098, Nanjing, China.

Submitted to

Composites Part B: Engineering

*Assistant Professor, e-mail: alfonso.pagani@polito.it
†PhD Student, e-mail: yanyanghhu@hhu.edu.cn
‡Professor of Aerospace Structures andAeroelasticity, e-mail: erasmo.carrera@polito.it

ABSTRACT

In the present work, a close-form solution based on a unified one-dimensional model is proposed and then applied to static response analyses of cross-ply laminated and sandwich beams subjected to simply supported boundary conditions. The hierarchical beam model is derived within the framework of the Carrera Unified Formulation (CUF), which makes use of Lagrange polynomials to express the three-dimensional (3D) displacement field via arbitrary order approximation of pure displacement variables at each layer over the cross section, in a Layer-Wise (LW) sense. The governing equations are derived via the principle of virtual work and a Navier-type close-form solution is employed to solve the resulting boundary value problem. Four benchmark numerical examples are carried out to demonstrate the efficiency of this novel method, including compact multi-layered cross-ply laminated beams, a thin-walled composite box beam and a composite sandwich-box beam. The results show that accurate displacement and stress components can be obtained as the order of the expansion increases, accompanied by a significant reduction in computational costs in comparison with the 3D finite element solutions. Besides, numerical cases in this research may be taken as benchmarks for future assessments in this field.

1 Introduction

In the past few years, laminated composite and sandwich beams have experienced a fast development in aerospace engineering due to their superior properties, i.e., high strength- and stiffness-to-weight ratios. These valuable properties will, in turn, give rise to more complicated structural design [1] than ordinary isotropic materials [2]. Therefore, more sophisticated models are needed so that the effect of anisotropy, fiber angle, laminate stacking sequence and different loading conditions on 3D displacements and stresses can be described accurately. Classical theories under the hypothesis outlined by Euler-Bernoulli (EB) and Timoshenko, also known as first-order shear deformation theory (FSDT), will result in inaccurate results because unable to give a correct transverse shear stress distribution along the thickness of the laminate.

In order to overcome this deficiency, several higher-order shear deformation theories (HSDT) were proposed accounting for the shear deformation effects, which can be classified into two categories: Equivalent Single Layer (ESL) and Layer-Wise theories. ESL theory assumes, at least, C^1 continuous displacements along the entire thickness direction. This assumption means that the number of unknowns is independent of the number of layers. Kant and Manjunath [3] presented a 2D higher-order theory for the analysis of laminated composite and sandwich beams, based on Taylor Expansion (TE) of the axial displacement. In [4], Zenkour used EB, Timoshenko and 2D higher-order theories for the bending analysis of laminated and sandwich beams. An extension of [3] was proposed by Reddy [5], who obtained 3D elasticity solutions of laminated composite plates by employing the TE of both in-plane displacements. Khedeir and Reddy [6] employed this theory in conjunction with the state-space concept to provide exact solutions of cross-ply laminated beams with arbitrary boundary conditions subjected to arbitrary loadings. Maiti and Sinha [7] developed a nine-node isoparametric element method for the bending and free vibration behaviour of angle-ply laminated composite beams, according to the full TE of all displacements. Aydogdu [8] and Karama et al. [9] presented a novel refined theory considering the exponential functions as higher-order terms in the displacement components to model the static and dynamic behaviour of multi-layered laminated composite beams. Other theories within the framework of the trigonometric shear deformation theories, which introduced a shear strain function in the displacement field through the thickness direction, can be found in [10, 11, 12, 13].

Although ESL exhibits a wide spectrum of application covering the static and dynamic analysis of composite beams, it lacks enough accuracy in predicting the shear stress at the layer interface due to the hypothesis of continuous derivatives of the displacements. In the recent literature, a LW model was proposed by Reddy [14] to remove this deficiency. In the domain of LW, a continuous displacement assumption is considered in each separate layer. It follows that C^0 continuous displacement assumption can be satisfied automatically. Pagano [15] used LW method for the cylindrical bending behaviour of 2D laminated structures and a close-form solution was obtained. Davalos et al. [16] applied FSDT in combination with LW method to obtain accurate stresses for each layer and interlaminar shear stresses via the parabolic interpolation strategy in a post-processing operation. Shimpi and Ainapure [17] presented a LW trigonometric shear deformation theory

for a two-layer laminated beam in which the sinusoidal function in terms of thickness coordinate was added to the displacement field for each layer, satisfying continuity of shear stress in the interface. The same theory was also utilized for the bending analysis of the sandwich beam under plane stress condition [18]. Tahani [19] developed two simplified LW theories for the static and dynamic properties of composite beam with general laminations and compared results with those of Pagano [15]. However, burdensome computation cost is required in this theory as the number of layers increases.

In the present work, exact LW solutions are obtained in the framework of the Carrera Unified Formulation, which was introduced by Carrera et al. [20, 21, 22] for the analysis of plate and shell structures and extended to the beams later. According to 1D CUF, the 3D displacement field can be approximated by any order of expansion functions over the cross section. The expansion order can be regarded as a free input parameter so that EB, FSDT and HSDT can be elegantly implemented hierarchically in a unified form. Four classes of CUF 1D models have been developed according to the different expansions adopted, which can be classified as follows: Taylor Expansion (TE), Lagrange Expansion (LE), Chebyshev Expansions (CE) and Hierarchical Legendre Expansion (HLE). Carrera et al. [23] presented 1D hierarchical beam elements, based on CUF TE method to analyze the bending and torsion behaviour of isotropic beams with arbitrary cross-section geometries. Catapano et al. [24] and Giunta et al. [25] proposed an extension of [23] to the static analysis of cross-ply laminated and sandwich beams in terms of ESL theory, respectively. Moreover, CUF TE method has also been applied to the free vibration analysis [26, 27, 28] and buckling phenomenon [29, 30] of laminated and sandwich beams with more complex material properties. Recently, Carrera and Petrolo [31] developed CUF LE method for the analysis of metallic as well as laminated and sandwich beams. Only unknown displacement variables are involved in this novel method so that this model is geometrically consistent and is prone to be implemented in a LW sense. As a result, CUF LE model has a great advantage over CUF TE in dealing with composite laminates. Carrera et al. [32, 33, 34] exploited computationally efficient elements in the light of CUF LE and TE methods for the static and free vibration analysis of laminated beams with compact and thin-walled sections. From the results, it can be seen that the use of CUF LE method permits the detection of more accurate shear stresses and higher modes than the employment of CUF TE method. Other information on CUF CE and HLE approaches can be found in [35, 36]. Most of the contributions on CUF LE method fall in the domain of the finite element method (FEM). Conversely, strong-form solutions may be desirable both in the case of both laminated composite structures and other applications, see for example [37, 38, 39]. Recently, Dan et al. [40] dealt with the linear vibration of isotropic beams with solid and thin-walled cross-sections through the Navier-type close-form solution and LE CUF models. Yan et al. [41],conversely, extended this methodology to the free vibration of composite beams.

Given the encouraging results of strong-form solutions based on CUF LE method, the present work provides the exact (in the framework of the proposed models) static response analyses and stress/strain distributions of laminated, box and sandwich beams with the simply supported boundary conditions. A brief outline of

the rest of this paper follows: an overview of anisotropic elasticity theory is introduced in Section 2, followed by a description of LW model within the framework of CUF LE in Section 3; in Section 4, the governing equations in strong form for the static analysis of laminated and sandwich beams are derived; Section 5 is devoted to the close-form solution application of CUF LE models. Four benchmark test problems are carried out to demonstrate the efficiencies of the proposed model. Some conclusions and remarks are provided in the last section.

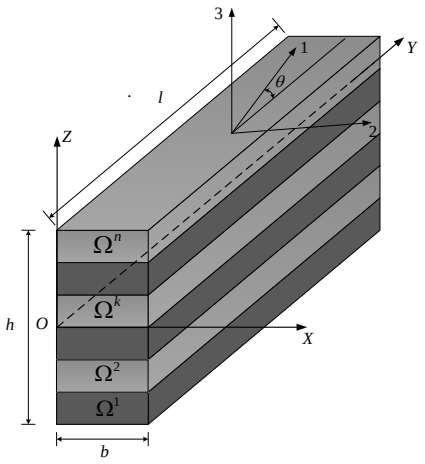

Figure 1: Geometry and reference coordinate systems for a multi-layered composite beam.

2 Preliminaries

Consider a multi-layered composite beam, with length l, width b and thickness h (Fig. 1). The y-axis is assumed to be placed on the longitudinal axis of the beam and xz-plane corresponds to the cross section Ω, being composed of Ω^k. Superscript k represents the layer index. For convenience, we will omit the parameter k in the following derivation. 3D displacement field in a given point of each kth-layer level is

$$\mathbf{u}(x,y,z) = \{u_x \ u_y \ u_z\}^{\mathrm{T}} \tag{1}$$

where u_x, u_y and u_z indicate the displacement components along three axes x, y, z, respectively. The index "T" denotes the transpose operator. The strain and stress tensors can be expressed in a vector forms, which read:

$$\boldsymbol{\sigma} = \{\sigma_{yy} \ \sigma_{xx} \ \sigma_{zz} \ \sigma_{xz} \ \sigma_{yz} \ \sigma_{xy}\}^{\mathrm{T}}, \quad \boldsymbol{\epsilon} = \{\epsilon_{yy} \ \epsilon_{xx} \ \epsilon_{zz} \ \epsilon_{xz} \ \epsilon_{yz} \ \epsilon_{xy}\}^{\mathrm{T}} \tag{2}$$

According to the small deformation assumption, the linear relation between strain $\boldsymbol{\epsilon}$ and displacement $\mathbf{u}$ components is given by:

$$\boldsymbol{\epsilon} = \mathbf{D}\mathbf{u} \tag{3}$$

where $\mathbf{D}$ is a 6×3 matrix, whose elements can be found in [31] for the sake of brevity. In the case of fiber-reinforced polymer-matrix composites, the material property of each laminae is assumed to be orthotropic in a material coordinate system (1,2,3), which does not always coincide with the global coordinate system (x, y, z). Thus, the monoclinic constitutive equation referred to the (x, y, z) coordinate system at layer level is developed as

$$\boldsymbol{\sigma} = \tilde{\mathbf{C}}\boldsymbol{\epsilon} \tag{4}$$

Coefficients in the matrix above can be computed by adequate coordinate transformations, which are expressions of three parameters: Young modulus, Poisson ratios and fiber orientation angle (θ) between the y and 1 axes, as shown in Fig. 1. For the sake of clarity, we do not provide their explicit forms, one can refer to Reddy [14] for further details.

3 Carrera Unified Formulation

CUF was proposed by Carrera [42] originally, who treated all the theories of structures in a single formulation. Accordingly, in the case of beam models, the generic displacement field can be expanded as arbitrary functions of the cross section, defined as:

$$\mathbf{u}(x, y, z) = F_\tau(x, z)\mathbf{u}_\tau(y) \qquad \tau = 1, 2, ..., M \tag{5}$$

where F_τ are functions of the x and z coordinates. $\mathbf{u}_\tau$ are the generalized displacements vector with respect to axial coordinates y. M stands for the number of expanded terms, and the repeated subscript, τ, stands for summation.

3.1 Layer-wise model based on CUF Lagrange expansion

CUF LE models can deal with LW approach elegantly by assuming the displacement function within each layer independently and imposing the displacement continuous condition at the layers interfaces. In detail, in the case of LE, the functions F_τ are defined as Lagrange polynomials for each layer in the natural coordinate system. Therefore, the arbitrarily shaped cross section can be dealt with easily by using different types of LE polynomials, which can be four-node bilinear L4, nine-node quadratic L9, and sixteen-node cubic L16. The

expression of a L9 polynomial is presented here as an illustrative example:

$$F_\tau = \tfrac{1}{4}(\mathrm{r}^2 + \mathrm{r}\ \mathrm{r}_\tau)(\mathrm{s}^2 + \mathrm{s}\ \mathrm{s}_\tau) \qquad \tau = 1,3,5,7$$

$$F_\tau = \tfrac{1}{2}\mathrm{s}_\tau^2(\mathrm{s}^2 - \mathrm{s}\ \mathrm{s}_\tau)(1 - r^2) + \tfrac{1}{2}\mathrm{r}_\tau^2(\mathrm{r}^2 - \mathrm{r}\ \mathrm{r}_\tau)(1 - \mathrm{s}^2) \qquad \tau = 2,4,6,8 \tag{6}$$

$$F_\tau = (1 - \mathrm{r}^2)(1 - \mathrm{s}^2) \qquad \tau = 9$$

where r and s vary over the interval $[-1, +1]$, and r_τ and s_τ indicate the vertex location in an isoparametric domain. For more details about the other two kinds of LE polynomials, interested readers can refer to Carrera and Petrolo [31].

The beam model with nine-node quadratic single-L9 kinematic field is given by the expression:

$$\begin{aligned} u_x &= F_1 u_{x_1} + F_2 u_{x_2} + F_3 u_{x_3} + F_4 u_{x_4} + F_5 u_{x_5} + F_6 u_{x_6} + F_7 u_{x_7} + F_8 u_{x_8} + F_9 u_{x_9} \\ u_y &= F_1 u_{y_1} + F_2 u_{y_2} + F_3 u_{y_3} + F_4 u_{y_4} + F_5 u_{y_5} + F_6 u_{y_6} + F_7 u_{y_7} + F_8 u_{y_8} + F_9 u_{y_9} \\ u_z &= F_1 u_{z_1} + F_2 u_{z_2} + F_3 u_{z_3} + F_4 u_{z_4} + F_5 u_{z_5} + F_6 u_{z_6} + F_7 u_{z_7} + F_8 u_{z_8} + F_9 u_{z_9} \end{aligned} \tag{7}$$

where $u_{x_1}, ..., u_{z_9}$ are the nine-node translational displacement variables of the problem considered.

It is worth mentioning that the proposed LE beam model can be refined by utilizing a combination of L9 kinematics on the sub-domain of each layer to the desired accuracy.

4 Principle of virtual work

Principle of virtual work in the case of static analysis can be expressed as:

$$\delta L_{\text{int}} - \delta L_{\text{ext}} = 0 \tag{8}$$

where δ is the symbol of a virtual variation. L_{int} stands for the strain energy, L_{ext} is the virtual work of the external loading.

The strain energy can be described as:

$$\delta L_{\text{int}} = \int_V \delta \boldsymbol{\epsilon}^{\mathrm{T}} \boldsymbol{\sigma} \mathrm{d}V \tag{9}$$

where V is the volume of the beam structure. By substitution of the geometrical relations (Eq. (3)), the constitutive equations (Eq. (4)) and CUF displacement field (Eq. (5)) and following integration by parts (see

[43]), Eq. (9) can be rewritten as:

$$\delta L_{\text{int}} = \int_l (\delta \boldsymbol{u}_\tau)^{\mathrm{T}} \mathbf{K}^{\tau s} \boldsymbol{u}_s \mathrm{d}y + \left[(\delta \boldsymbol{u}_\tau)^{\mathrm{T}} \boldsymbol{\Pi}^{\tau s} \boldsymbol{u}_s\right] |_{y=0}^{y=l} \tag{10}$$

where $\mathbf{K}^{\tau s}$ is 3×3 fundamental nucleus of the stiffness matrices and $\boldsymbol{\Pi}^{\tau s}$ represents the matrix of the boundary conditions . The explicit expressions concerning these fundamental nuclei are not reported here for the sake of brevity. It can be found in [26]. Moreover, it should be noted that the term $\left[(\delta \boldsymbol{u}_\tau)^{\mathrm{T}} \boldsymbol{\Pi}^{\tau s} \boldsymbol{u}_s\right] |_{y=0}^{y=l}$ is equal to zero in the case of simply supported beams and will be removed in the following derivation.

The virtual variation of the external work by a surface loading $(p_{ij}, i, j = x, y, z)$ acting on the nth sub-domain on the cross section (see Fig. 2) is:

$$\delta L_{\text{ext}} = \left(\delta L^n_{p^{\pm}_{xx}} + \delta L^n_{p^{\pm}_{xy}} + \delta L^n_{p^{\pm}_{xz}} + \delta L^n_{p^{\pm}_{zx}} + \delta L^n_{p^{\pm}_{zy}} + \delta L^n_{p^{\pm}_{zz}}\right) \tag{11}$$

Where:

$$\delta L^n_{p^{\pm}_{zz}} = \int_l \delta u_{z\tau} p^{n\pm}_{zz} E^{nx^{\pm}}_{\tau}\ dy, \quad \left(E^{nx^{+}}_{\tau}, E^{nx^{-}}_{\tau}\right) = \int_{x_1^n}^{x_2^n} \left(F_\tau\left(z_2^n, x\right), F_\tau\left(z_1^n, x\right)\right)\ dx \tag{12}$$

$\left[z_1^k, z_2^k\right]$ represent the z coordinates of the bottom and upper surfaces, respectively. The explicit expressions of the other components in Eq. (11) can be found in [42].

Substituting Eq. (11) into Eq. (8) and assuming orthotropic laminates, the explicit form of the governing

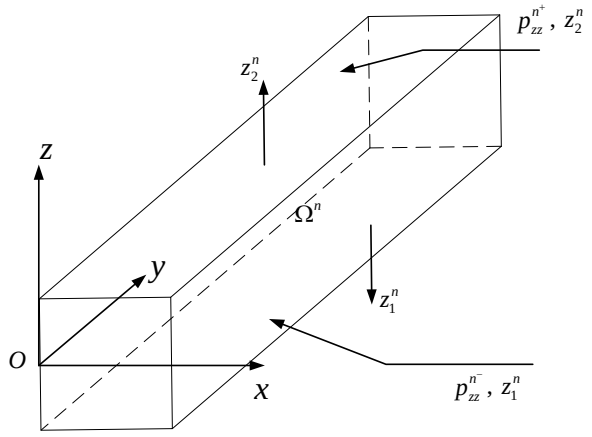

Figure 2: Surface load $p^{n\pm}_{zz}$ and its normal vectors.

equations can be written in the following unified form:

$$
\begin{aligned}
\delta u_{x\tau}: \quad & -E^{66}_{\tau s}u_{xs,_{yy}} + \big(E^{26}_{\tau,_x s} - E^{26}_{\tau s,_x}\big)u_{xs,_y} + \big(E^{22}_{\tau,_x s,_x} + E^{44}_{\tau,_z s,_z}\big)u_{xs} \\
& -E^{36}_{\tau s}u_{ys,_{yy}} + \big(E^{23}_{\tau,_x s} - E^{66}_{\tau s,_x}\big)u_{ys,_y} + \big(E^{26}_{\tau,_x s,_x} + E^{45}_{\tau,_z s,_z}\big)u_{ys} \\
& +\big(E^{45}_{\tau,_z s} - E^{16}_{\tau s,_z}\big)u_{zs,_y} + \big(E^{44}_{\tau,_z s,_x} + E^{12}_{\tau,_x s,_z}\big)u_{zs} = \Big(p^{n\pm}_{xx}E^{nz^{\pm}}_{\tau} \\
& +p^{n\pm}_{zx}E^{nx^{\pm}}_{\tau}\Big) \\
\delta u_{y\tau}: \quad & -E^{36}_{\tau s}u_{xs,_{yy}} + \big(E^{66}_{\tau,_x s} - E^{23}_{\tau s,_x}\big)u_{xs,_y} + \big(E^{26}_{\tau,_x s,_x} + E^{45}_{\tau,_z s,_z}\big)u_{xs} \\
& -E^{33}_{\tau s}u_{ys,_{yy}} + \big(E^{36}_{\tau,_x s} - E^{36}_{\tau s,_x}\big)u_{ys,_y} + \big(E^{66}_{\tau,_x s,_x} + E^{55}_{\tau,_z s,_z}\big)u_{ys} \\
& +\big(E^{55}_{\tau,_z s} - E^{13}_{\tau s,_z}\big)u_{zs,y} + \big(E^{16}_{\tau,_x s,_z} + E^{45}_{\tau,_z s,_x}\big)u_{zs} = \Big(p^{n\pm}_{zy}E^{nx^{\pm}}_{\tau} \\
& +p^{n\pm}_{xy}E^{nz^{\pm}}_{\tau}\Big) \\
\delta u_{z\tau}: \quad & \big(E^{16}_{\tau,_z s} - E^{45}_{\tau s,_z}\big)u_{xs,_y} + \big(E^{44}_{\tau,_x s,_z} + E^{12}_{\tau,_z s,_x}\big)u_{xs} \\
& +\big(E^{13}_{\tau,_z s} - E^{55}_{\tau s,_z}\big)u_{ys,_y} + \big(E^{45}_{\tau,_x s,_z} + E^{16}_{\tau,_z s,_x}\big)u_{ys} - E^{55}_{\tau s}u_{zs,_{yy}} \\
& +\big(E^{45}_{\tau,_x s} - E^{45}_{\tau s,_x}\big)u_{zs,_y} + \big(E^{44}_{\tau,_x s,_x} + E^{11}_{\tau,_z s,_z}\big)u_{zs} = \Big(p^{n\pm}_{zz}E^{nx^{\pm}}_{\tau} \\
& +p^{n\pm}_{xz}E^{nz^{\pm}}_{\tau}\Big)
\end{aligned}
\tag{13}
$$

where the suffix after the comma indicates the derivatives and the generic term $E^{\alpha\beta}_{\tau,_\theta s,_\zeta}$ is a cross-sectional moment parameter:

$$
E^{\alpha\beta}_{\tau,_\theta s,_\zeta} = \int_{\Omega} \tilde{C}_{\alpha\beta}F_{\tau,_\theta}F_{s,_\zeta}\mathrm{d}\Omega \tag{14}
$$

It should be noted that Eq. (13) represents a system of governing equations that are valid for any beam theory. By expanding the governing equations according to the indexes τ and s, any beam model can be formulated with ease.

5 Analytical solution

The analytical solution of the above governing equations is possible to be solved via a Navier-type, close-form solution under simply supported boundary conditions. The displacement fields and transverse surface load can be expanded as the following Fourier series:

$$\begin{aligned} u_{x\tau}(y) &= U_{x\tau}\sin(\alpha y) \\ u_{y\tau}(y) &= U_{y\tau}\cos(\alpha y) \\ u_{z\tau}(y) &= U_{z\tau}\sin(\alpha y) \end{aligned} \tag{15}$$

where α is:

$$\alpha = \frac{m\pi}{l} \tag{16}$$

and $U_{x\tau}$, $U_{y\tau}$ and $U_{z\tau}$ are amplitudes of the generalized displacements vector. m is the half wave number along the beam axis.

Accordingly, the surface load can be expressed as

$$\mathbf{p}^n = \left\{ \begin{array}{l} p_{xx}^{n\pm}\sin(\alpha y) \\ p_{xy}^{n\pm}\cos(\alpha y) \\ p_{xz}^{n\pm}\sin(\alpha y) \\ p_{zx}^{n\pm}\sin(\alpha y) \\ p_{zy}^{n\pm}\cos(\alpha y) \\ p_{zz}^{n\pm}\sin(\alpha y) \end{array} \right\} \tag{17}$$

Substituting Eq. (15) and Eq. (17) into Eq. (13) and after simplifications, it reads:

$$\mathbf{K}^{\tau s}\boldsymbol{U}_s = \mathbf{P}^{\tau} \tag{18}$$

where

$$
\begin{aligned}
&K_{xx}^{\tau s}=\alpha^{2} E_{\tau s}^{66}+E_{\tau_{,x} s_{,x}}^{22}+E_{\tau_{,z} s_{,z}}^{44}, K_{xy}^{\tau s}=-\alpha\left(E_{\tau_{,x} s}^{23}-E_{\tau s_{,x}}^{66}\right), K_{xz}^{\tau s}=E_{\tau_{,z} s_{,x}}^{44}+E_{\tau_{,x} s_{,z}}^{12} \\
&K_{yx}^{\tau s}=\alpha\left(E_{\tau_{,x} s}^{66}-E_{\tau s_{,x}}^{23}\right), K_{yy}^{\tau s}=\alpha^{2} E_{\tau s}^{33}+E_{\tau_{,x} s_{,x}}^{66}+E_{\tau_{,z} s_{,z}}^{55}, K_{yz}^{\tau s}=\alpha\left(E_{\tau_{,z} s}^{55}-E_{\tau s_{,z}}^{13}\right) \\
&K_{zx}^{\tau s}=E_{\tau_{,x} s_{,z}}^{44}+E_{\tau_{,z} s_{,x}}^{12}, K_{zy}^{\tau s}=-\alpha\left(E_{\tau_{,z} s}^{13}-E_{\tau s_{,z}}^{55}\right), K_{zz}^{\tau s}=\alpha^{2} E_{\tau s}^{55}+E_{\tau_{,x} s_{,x}}^{44}+E_{\tau_{,z} s_{,z}}^{11} \\
&P_{x}^{\tau s}=p_{xx}^{n \pm} E_{\tau}^{n z^{\pm}}+p_{z x}^{n \pm} E_{\tau}^{n x^{\pm}}, P_{y}^{\tau s}=p_{z y}^{n \pm} E_{\tau}^{n x^{\pm}}+p_{x y}^{n \pm} E_{\tau}^{n z^{\pm}}, P_{z}^{\tau s}=p_{z z}^{n \pm} E_{\tau}^{n x^{\pm}}+p_{x z}^{n \pm} E_{\tau}^{n z^{\pm}}
\end{aligned}
\tag{19}
$$

Eq. (18) is written at the layer level and can be assembled into a global algebraic eigensystem using LW

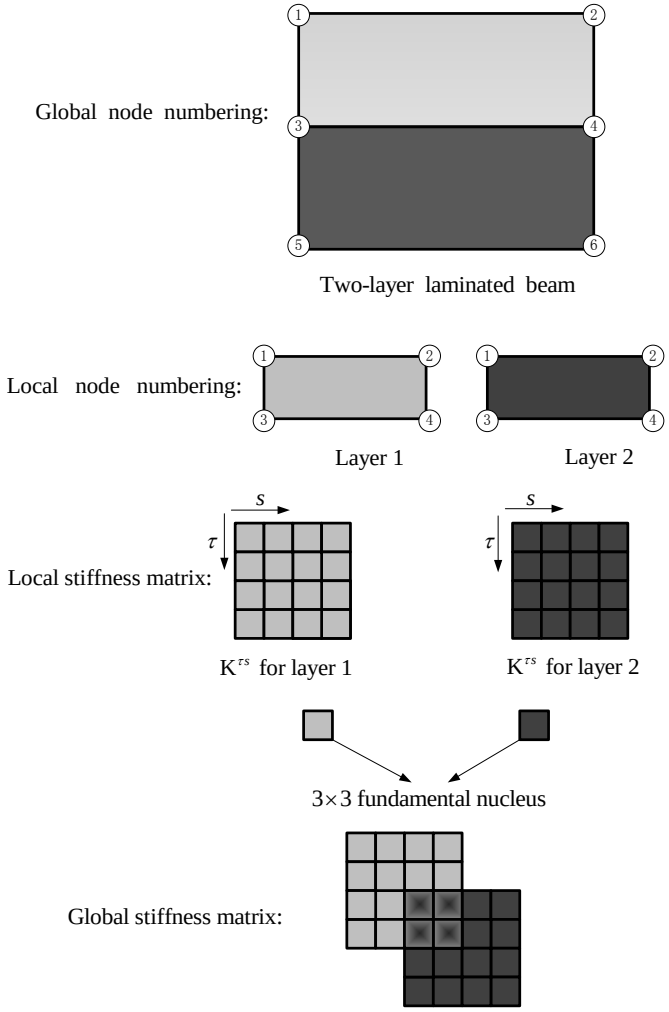

Figure 3: Assembly process of the local stiffness matrices in a two-layer laminated beam via LW theory.

approach. To be specific, the local stiffness and mass matrices of the Eq.(18) can be assembled into a global matrices by considering the contribution of each layer and the continuity of the displacement solutions at the intra-layer interfaces can be assured by the superposition of the related matrix elements of shared nodes in separate domains, as shown in Fig. 3. Eventually, higher-order LW models can be easily achieved by increasing the order of LE expansions at each layer to the desired accuracy.

6 Numerical results

In order to evaluate the accuracy of the proposed CUF-LE beam model, numerical examples of static analysis on simply-supported cross-ply composite beams subject to sinusoidal transverse loading are presented in this section. Laminated beams with compact square cross-section are employed for the preliminary assessments, in which both symmetric and anti-symmetric stacking sequences are considered. The remaining two examples are further performed on the thin-walled composite box beam and composite sandwich-box beam.

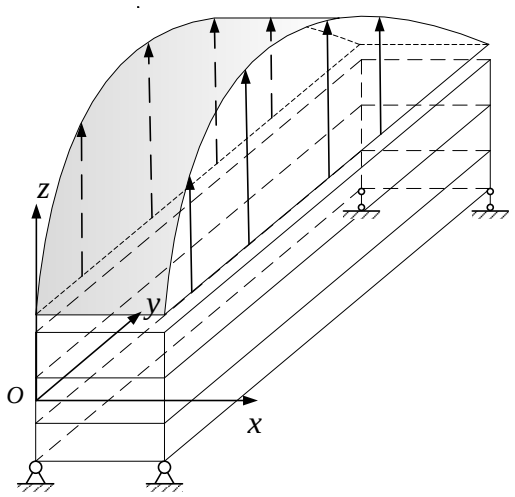

Figure 4: A three-layer composite beam under sinusoidal pressure load.

6.1 Symmetric cross-ply laminated beams

The first assessment is carried out for a three-layered $[0°/90°/0°]$ laminated beam. Its geometry parameters are chosen as: width, $b = 0.2$m, height, $h = 0.2$m, and length-to-width ratio, $l/b = 10$m. Each lamina is of equal thickness and composed of an orthotropic material with the following properties in the fiber longitudinal and transverse direction: Young moduli: $E_L = 250$ GPa, $E_T = 10$ GPa; Poisson ratios: $\nu_{LT} = \nu_{TT} = 0.25$. The transverse sinusoidal loading is applied to the upper surface in terms of $p(y) = p_0 \sin\frac{\pi y}{l}$ with p_0 equal to unity, see Fig. 4. All the results are given in the following dimensionless form:

$$\bar{u}_i = \frac{E_T}{h} u_i \quad \text{with} \quad i = x, y; \quad \bar{u}_z = 100\frac{E_T h^3}{l^4} u_z$$
$$\bar{\sigma}_{ij} = \frac{\sigma_{ij}}{p_0} \quad \text{with} \quad i = x, y, z; \quad \bar{z} = \frac{z}{h} \tag{20}$$

where $\bar{u}_i$ and $\bar{\sigma}_{ij}$ stands for the dimensionless displacement and stress components.

Table 1: Non-dimensional displacement and stress results for a three-layer composite beam [0°/90°/0°] under sinusoidal surface loading, $l/b = 10$.

	$\bar{u}_z$	$\bar{u}_y$	$\bar{\sigma}_{yy}$		$\bar{\sigma}_{yz}$	DOFs
Model	$[0, l/2, -h/2]$	$[0, 0, -h/2]$	$[0, l/2, -h/2]$	$[0, l/2, h/2]$	$[0, 0, -h/4]$	
Reference solutions						
ESCBP [15]	0.920	-9.300	-73.200	73.200	4.100	–
BLWT [19]	0.900	–	–	–	–	–
FEM 3D[a]	0.931	-9.309	-73.520	73.462	3.801	197496
Present LE models						
1×6 L4	0.928	-9.253	-72.970	72.998	3.721	42
2×6 L4	0.928	-9.253	-72.971	73.009	3.714	63
1×6 L9	0.933	-9.349	-73.650	73.687	3.702	117
2×6 L9	0.933	-9.349	-73.652	73.684	3.703	195
1×3 L16	0.934	-9.350	-73.654	73.686	3.747	120
1×6 L16	0.934	-9.350	-73.651	73.689	3.763	228
2×6 L16	0.934	-9.350	-73.654	73.696	3.763	399

[a]: The number of elements is $15 \times 40 \times 15$

Table 1 shows the non-dimensional displacement and stress values measured at different locations for $l/b = 10$ by using a number of LE models, which can be expressed in a general form as $\zeta \times \eta \mathrm{L}\beta$, while $\vartheta \mathrm{L}\beta$ to denote those of thin-walled cross sections, where ζ and η stand for the number of Lβ elements in the x direction and z direction, ϑ stands for the number of Lβ elements over the whole cross section and β stands for the order of Lagrange polynomials. The Exact Solution for the Cylindrical Bending of Plates (ESCBP) developed by Pagano [15], the Beam Layer-Wise Theory (BLWT) employed by Tahani [19] and the ABAQUS model utilizing brick element C3D20 are also given in the same table for comparison purposes along with degrees of freedoms (DOFs) for each model. Out of these results, it can be observed that all the LE models can provide closer displacements and stresses solutions to 3D FEM model than ESCBP and BLWT models with less amount of computational cost. The maximum difference between 2×6 L16 models and 3D FEM model occurs for the axial displacement $\bar{u}_y$ (0.44%) and the transverse shear stress $\bar{\sigma}_{yz}$ (1.00%).

The non-dimensional transverse displacement, $\bar{u}_z$, axial displacement, $\bar{u}_y$, axial stress, $\bar{\sigma}_{yy}$ and transverse shear stress, $\bar{\sigma}_{yz}$ evaluated along the z-axis at the mid-span and the left end are displayed in Fig. 5 and Fig. 6, respectively. Bilinear, quadratic and third-order LE models and ABAQUS models are shown. It is obvious that the axial displacement and both of the stresses provided by LE models are in perfect agreement with ABAQUS models regardless of the expansion orders, with the exception of lower transverse displacement in 1×6 L4 model. Moreover, the proposed models carry with them the capability to account for zig-zag phenomena in displacements, interface discontinuity in in-plane axial stress and stress-free boundary conditions in out-of-plane transverse shear stress.

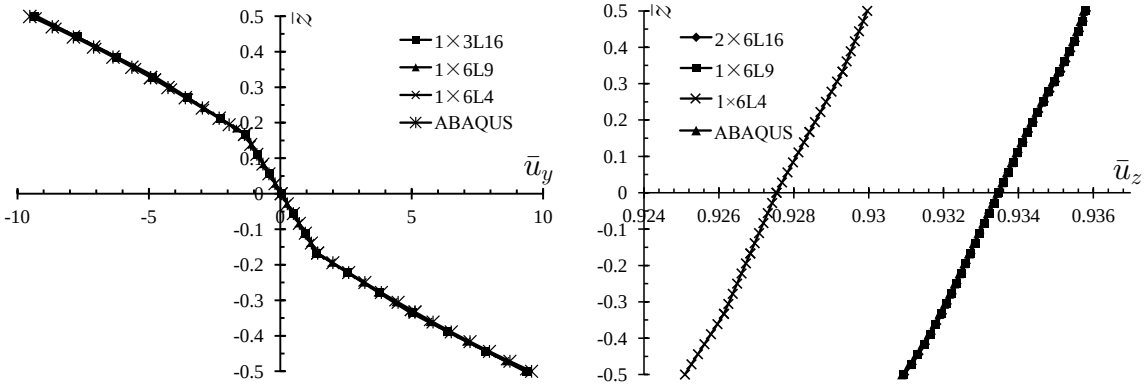

(a) $\bar{u}_y$ at $(x, y) = (0, 0)$ (b) $\bar{u}_z$ at $(x, y) = (0, l/2)$

Figure 5: Non-dimensional axial displacement, $\bar{u}_y$ and transverse displacement, $\bar{u}_z$ for the three-layer composite beam.

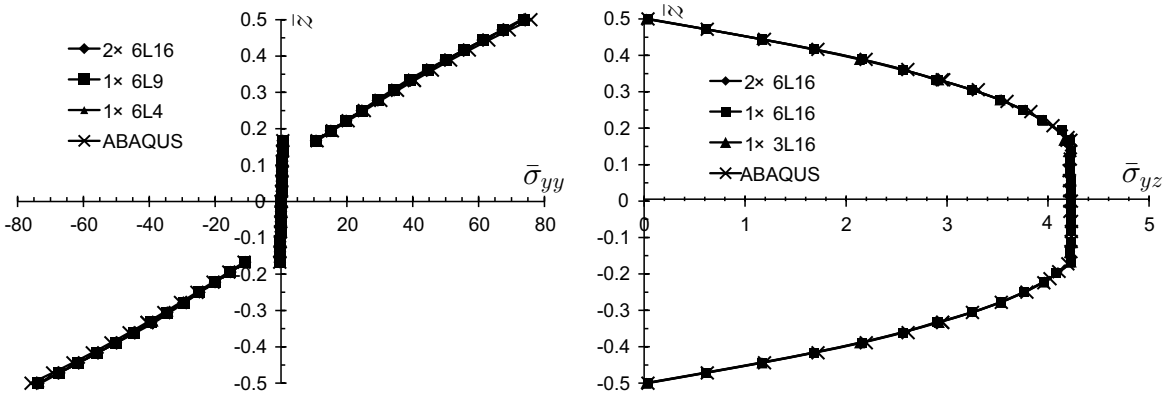

(a) $\bar{\sigma}_{yy}$ at $(x, y) = (0, l/2)$ (b) $\bar{\sigma}_{yz}$ at $(x, y) = (0, 0)$

Figure 6: Non-dimensional axial stress, $\bar{\sigma}_{yy}$ and transverse shear stress, $\bar{\sigma}_{yz}$ for the three-layer composite beam.

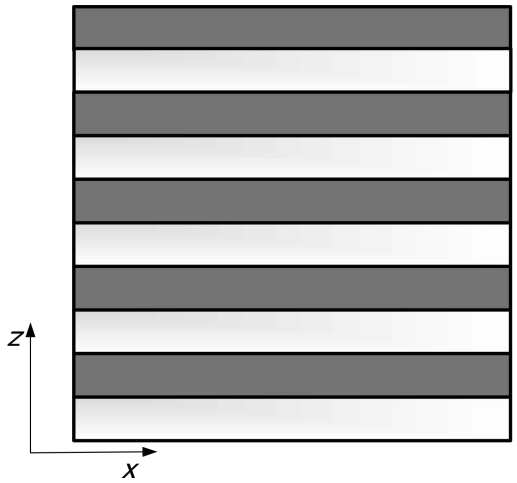

Figure 7: The cross-section for a ten-layer composite beam.

6.2 Anti-symmetric cross-ply laminated beams

An anti-symmetric cross-ply composite beam with ten layers is considered in the second case with $l/b = 10$ and cross section as shown in Fig. 7. The overall geometry, material properties and load magnitude remain the same as those in the previous case. Table 2 displays the transverse displacement $\bar{u}_z$ and transverse shear stress $\bar{\sigma}_{yz}$, and axial displacement $\bar{u}_y$ and axial stress $\bar{\sigma}_{yy}$, at different points. LE models and 3D FEM solutions are also provided here for comparison purposes. It is clear that higher-order LE models (L16) can produce more accurate results in terms of displacements and stresses than lower-order LE models (L4) in comparison with 3D FEM solutions. Less than 0.40% maximum relative error occurs for all expansion orders in regard to both displacements and stresses, being fewer DOFs than those of 3D FEM model.

Table 2: Non-dimensional displacement and stress results of the ten-layer composite beam, $l/b = 10$

Model	$\bar{u}_y$ $[0, 0, h/2]$	$\bar{u}_z$ $[0, l/2, -h/2]$	$\bar{\sigma}_{yy}$ $[0, l/2, h/2]$	$\bar{\sigma}_{yz}$ $[0, 0, h/4]$	DOFs
$2 \times$ 10L4	-18.54	1.403	6.116	3.229	99
$1 \times$ 10L9	-18.61	1.407	6.100	3.231	189
$5 \times$ 10L9	-18.61	1.408	6.115	3.231	693
$1 \times$ 10L16	-18.61	1.408	6.100	3.231	372
$5 \times$ 10L16	-18.61	1.408	6.078	3.232	1488
FEM 3D[a]	-18.61	1.406	6.093	3.234	262143

[a]: The number of elements is $20 \times 50 \times 20$

The non-dimensional displacement and stress variables along z at the middle and left border cross sections are illustrated in Fig. 8 and Fig. 9, respectively. As we can see, LE models can yield accurate results of $\bar{u}_y$ and $\bar{\sigma}_{yy}$ in comparison with the corresponding ABAQUS results for all the expansion orders considered, being less zig-zag behaviour for $\bar{u}_y$ (see Fig. 8(a)) and prominent discontinuousness for $\bar{\sigma}_{yy}$ (see Fig. 9(a)). Moreover, $\bar{u}_z$ is underestimated by the lower-order LE model ($2 \times$ 10L4) and reaches a higher value as the

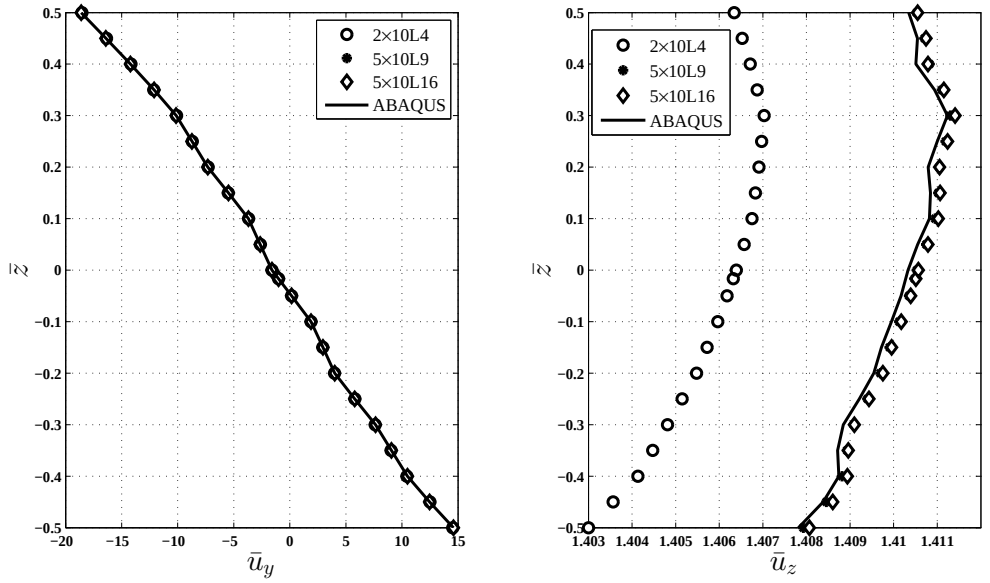

(a) $\bar{u}_y$ at $(x, y) = (0, 0)$ (b) $\bar{u}_z$ at $(x, y) = (0, l/2)$

Figure 8: Non-dimensional axial displacement, $\bar{u}_y$ and transverse displacement, $\bar{u}_z$ for the ten-layer composite beam.

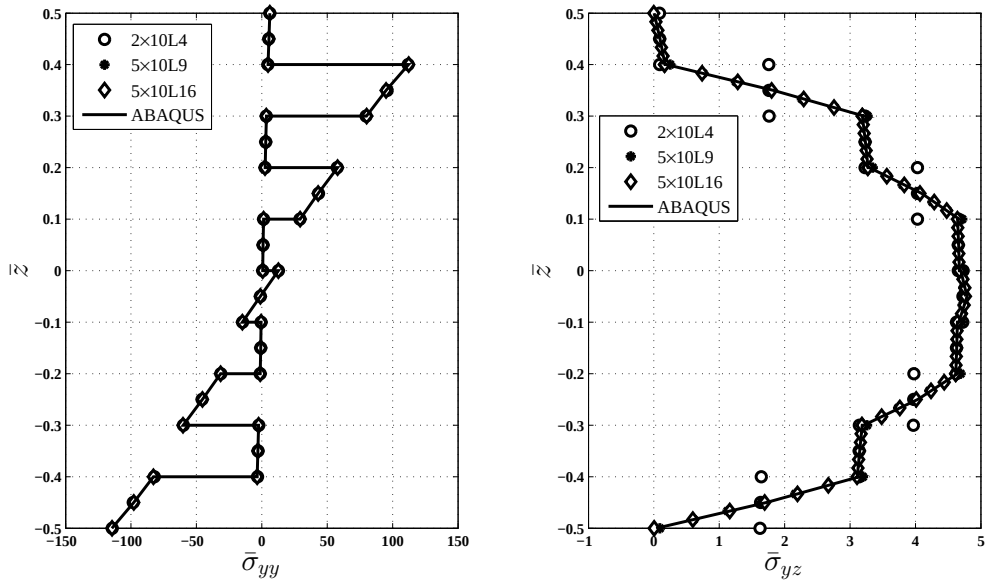

(a) $\bar{\sigma}_{yy}$ at $(x, y) = (0, l/2)$ (b) $\bar{\sigma}_{yz}$ at $(x, y) = (0, 0)$

Figure 9: Non-dimensional axial stress, $\bar{\sigma}_{yy}$ and transverse shear stress, $\bar{\sigma}_{yz}$ for the ten-layer composite beam.

expansion order increases, with ABAQUS result considered as a reference (see Fig. 8(b)). In Fig. 9(b), the lower-order LE model has also been proved to be incapable of obtaining the correct $\bar{\sigma}_{yz}$ at the interface, which is continuous in higher-order LE models.

6.3 Thin-walled composite box beam

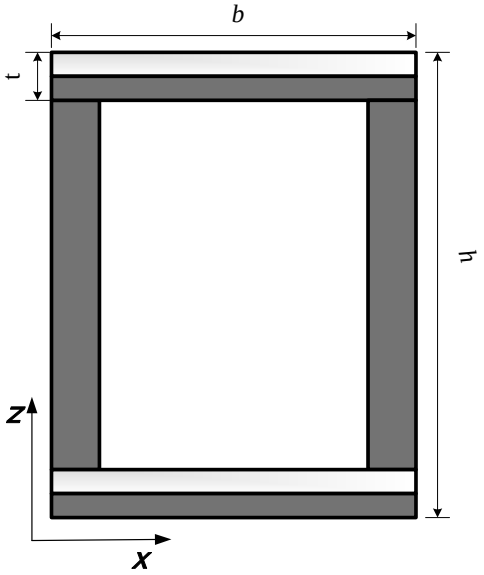

Figure 10: The cross-section for a single-bay composite box beam.

To test the applicability of the proposed models on the thin-walled composite beam, we consider a composite box beam with the following geometry: width $b = 0.1$m, height $h = 0.2$m, slenderness ratio $l/b = 10$. The flange and web have the same thickness: t=0.01m, but are composed of different laminations: [0°/90°] for the flange and [0°] for the web. An orthotropic material is used, whose properties are defined as: $E_L = 144$ MPa, $E_T = 9.65$ MPa, $G_{LT} = 4.14$ MPa, $G_{TT} = 3.45$ MPa, $\nu_{LT} = \nu_{LT}$=0.3, $\rho = 1389$ kg/m^3. A transverse sinusoidal loading is applied on the upper surface in terms of $p(y) = 10000 \sin \frac{\pi y}{l}$.

Table 3: Displacement and stress components of the single-bay composite box beam, $l/b = 10$

Model	$u_y \times 10^5$ (m) $[0, 0, h/2]$	$u_z \times 10^5$ (m) $[0, l/2, -h/2]$	$\sigma_{yy} \times 10^4$ (Pa) $[0, l/2, h/2]$	$\sigma_{yz} \times 10^4$ (Pa) $[0, 0, 3 \times h/20]$	DOFs
32L4	-0.1450	1.036	4.733	10.29	168
26L9	-0.1477	1.050	4.731	10.28	420
32L9	-0.1480	1.050	4.738	9.972	528
32L16	-0.1480	1.051	4.566	9.867	1062
FEM 3D[a]	-0.1480	1.052	4.743	9.873	336996

[a]: The number of elements in each flange is $24 \times 50 \times 6$,
The number of elements in each web is $3 \times 50 \times 30$.

The solutions of displacements and stresses computed by LE models with different expansion orders are listed in Table 3 and are compared with those from ABAQUS models, which come from convergence analysis for the purpose of a fair comparison. From the results of this table, a perfect correlation between LE and ABAQUS models, especially in terms of displacements, can be seen. It is also observed that LE models provide exact and convergent results with respect to the increasing expansion orders, with the exception of the maximum discrepancy (3.73%) in σ_{yy}.

Fig. 11 and Fig. 12 show the distribution of displacements and stresses in the representative location. Regarding these figures, the enhanced capability of higher-order LE models is evident once again. Different from previous two cases, the parabolic distribution of u_y, σ_{yy} and σ_{yz} for the web along z-axis can be captured. A more detailed description of the three-dimensional distribution of the corresponding variables are shown in Fig. 13. It is possible to see that the prominent deformation of u_z near mid-span, significant σ_{yy} near the bottom and top of the web, and concentrating σ_{yz} around both ends of the web.

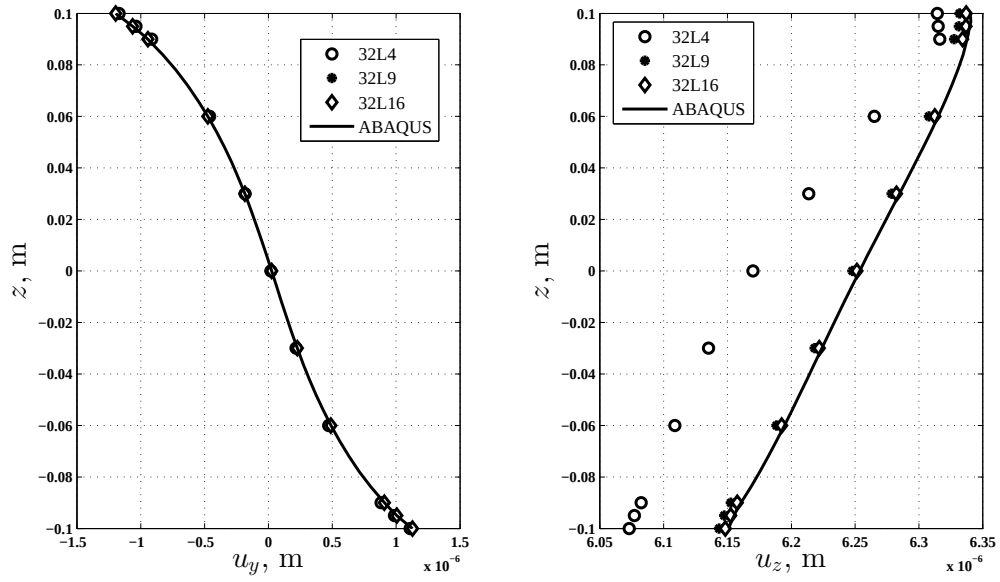

(a) u_y at $(x, y) = (b/30, l/5)$ (b) u_z at $(x, y) = (b/30, l/5)$

Figure 11: Axial displacement, u_y and transverse displacement, u_z along the thickness of the single-bay composite box beam.

6.4 Composite sandwich-box beam

To examine the applicability of the proposed LE beam model to real 3D problems, the last case of this section is a composite sandwich-box structure, as shown in Fig. 14. The geometric feature and loading case are assumed to be same as the one in the previous case and with $l/b = 5$. The material properties in the material

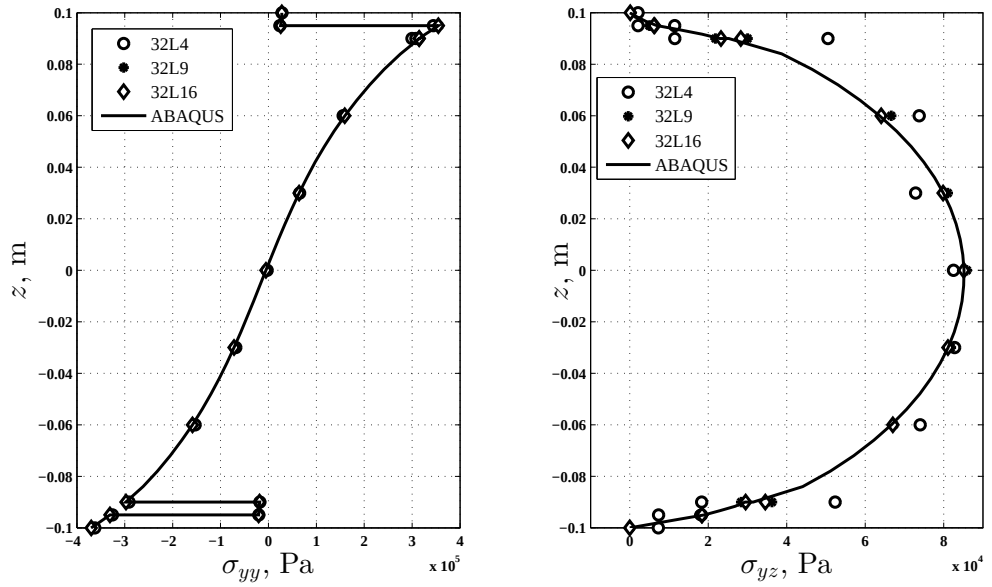

(a) σ_{yy} at $(x, y) = (b/30, l/5)$ (b) σ_{yz} at $(x, y) = (b/30, l/5)$

Figure 12: Non-dimensional axial stress, σ_{yy} and transverse shear stress, σ_{yz} along the thickness of the single-bay composite box beam.

Table 4: Material properties for core and face

	Core	Face
E_1 (Mpa)	0.2208	131100
E_2 (Mpa)	0.2001	6900
E_3 (Mpa)	2760	6900
G_{12} (Mpa)	16.56	3588
G_{23} (Mpa)	455.4	2332.2
G_{13} (Mpa)	545.1	3088
ν_{12}	0.99	0.32
ν_{23}	0.00003	0.49
ν_{13}	0.00003	0.32
ρ (kg/m^3)	70	1000

coordinate system (1, 2, 3) are given in Table 4.

Table 5 presents the values of displacements and stresses on different points, obtained via various LE and ABAQUS models. It can be seen that all LE models can provide exact u_y, u_z and σ_{yy} values, getting closer to ABAQUS results with lower computational cost, while regarding u_x and σ_{yz}, lower-order LE model (5×10L4) encounters a significant drop in solution accuracy. On the other hand, higher-order model (6×8L16) may produce non-negligible errors with respect to u_x and σ_{yz}, being 0.80% and 0.29% in comparison with ABAQUS results.

Fig. 15 and Fig. 16 show the distribution of displacements and stresses at the left end and mid-span. Out of these figures, piecewise linearity behaviour occurs for the case of u_y, σ_{yy} and σ_{yz}, while a parabolic distribution of u_z is presented on the web along z, which proves the exact opposite of the previous case. Furthermore, the core addresses the negligible σ_{yy} becoming closer to zero and the maximum σ_{yz} exactly when expansion order increases. Fig. 17 compares the three-dimensional representation of displacement and

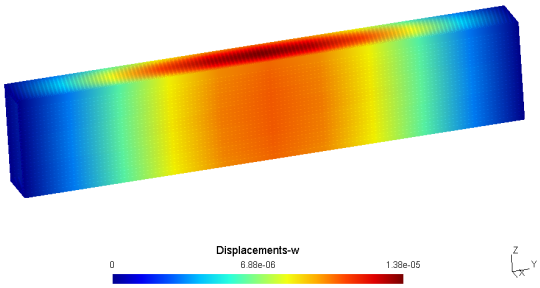

(a) 32L16, u_z

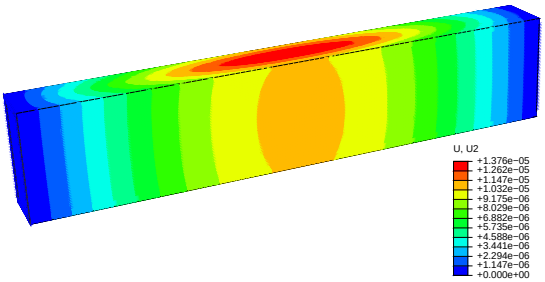

(b) ABAQUS, u_z

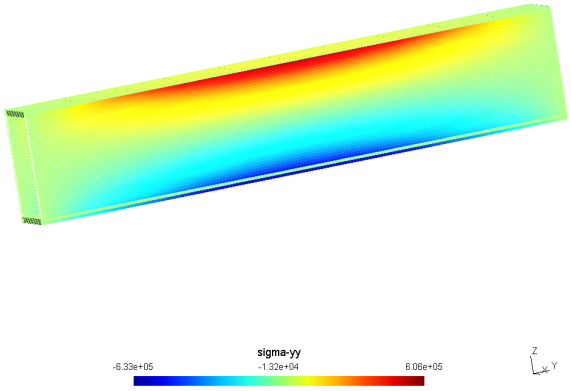

(c) 32L16, σ_{yy}

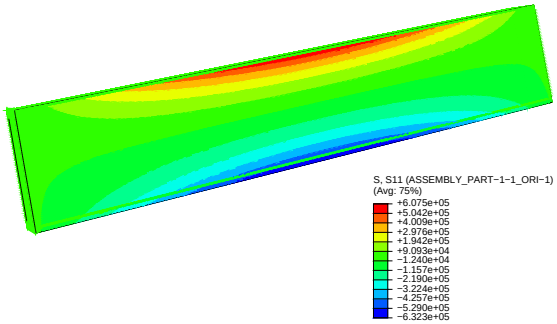

(d) ABAQUS, σ_{yy}

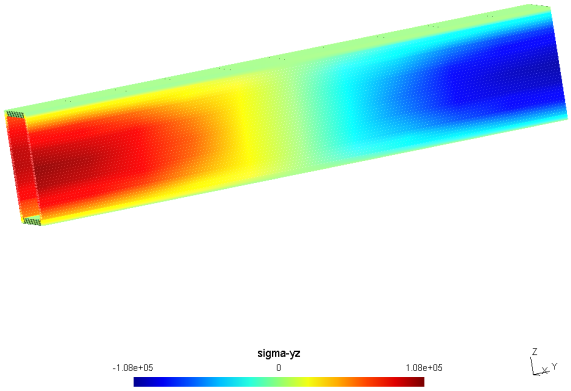

(e) 32L16, σ_{yz}

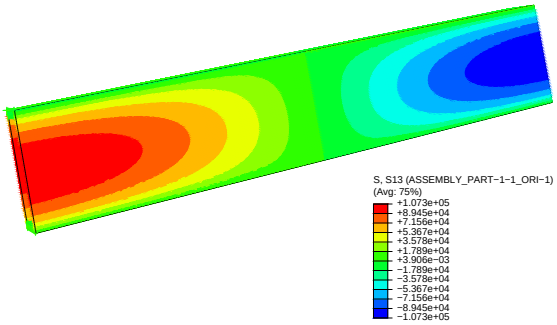

(f) ABAQUS, σ_{yz}

Figure 13: Comparison of the transverse displacement, u_z, the axial stress, σ_{yy} and transverse shear stress, σ_{yz}, by 32L16 and 3D FEM model.

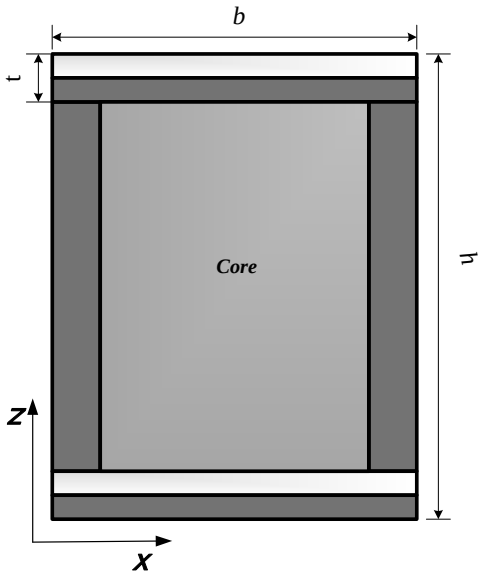

Figure 14: The cross-section for a composite sandwich-box beam.

Table 5: Displacement and stress components of the composite sandwich-box beam, $l/b = 5$

Model	$u_x \times 10^7$ (m) $[b, l/2, 0]$	$u_y \times 10^6$ (m) $[b, 0, h/2]$	$u_z \times 10^6$ (m) $[b, l/2, 0]$	$\sigma_{yy} \times 10^-5$ (Pa) $[0, l/2, -h/2]$	$\sigma_{yz} \times 10^-4$ (Pa) $[0, 0, 0]$	DOFs
5×10L4	-1.567	-1.497	9.379	-5.929	6.368	198
5×7L9	-2.258	-1.517	9.441	-5.996	6.428	495
5×10L9	-2.250	-1.519	9.447	-6.006	6.661	693
6×8L16	-2.266	-1.521	9.452	-6.008	6.588	1425
FEM 3D[a]	-2.248	-1.520	9.451	-6.006	6.607	262143

[a]: The number of elements is $20 \times 50 \times 20$

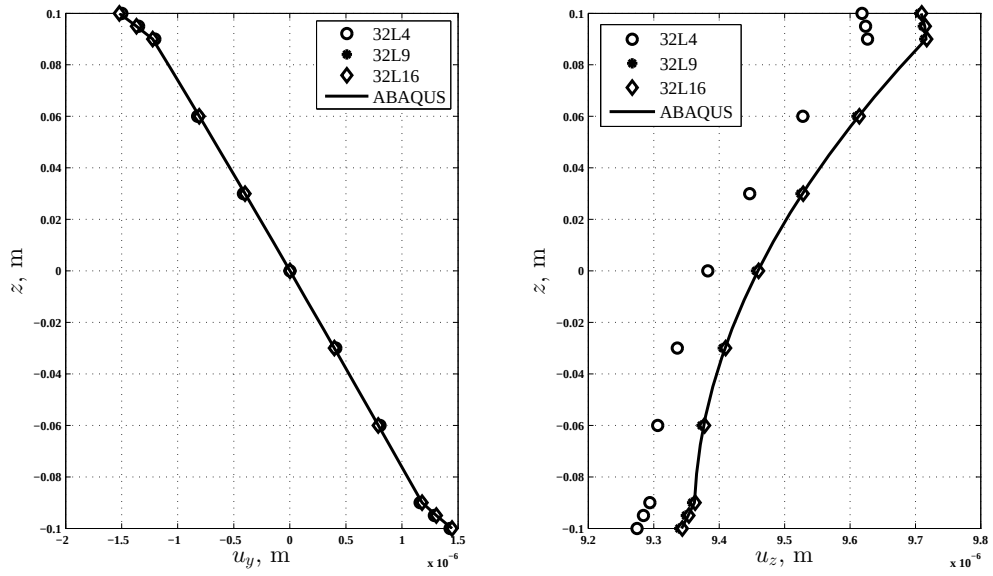

(a) u_y at $(x, y) = (b/2, l/2)$ (b) u_z at $(x, y) = (b/2, 0)$

Figure 15: Axial displacement, u_y and transverse displacement, u_z along the thickness of the composite sandwich-box beam.

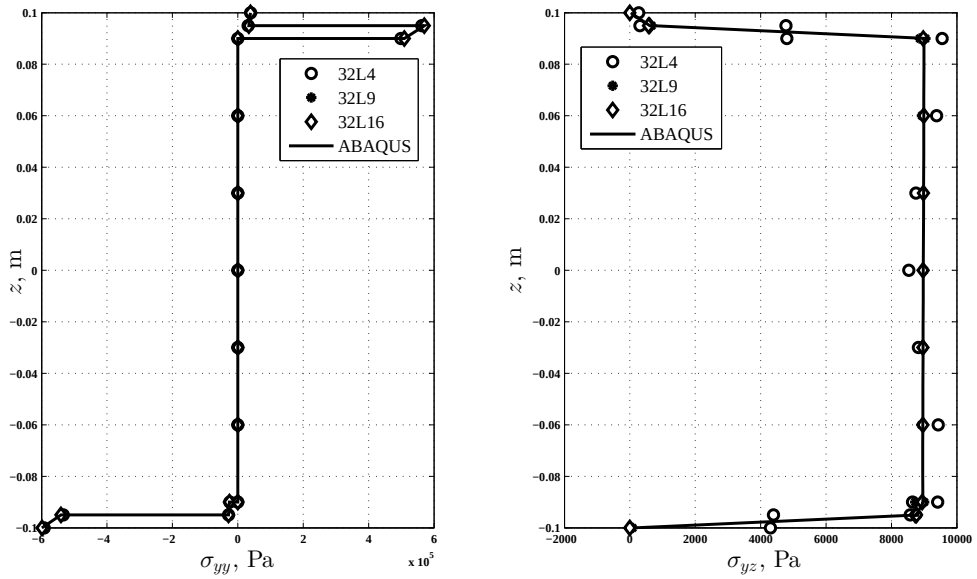

(a) σ_{yy} at $(x, y) = (b/2, l/2)$

(b) σ_{yz} at $(x, y) = (b/2, 0)$

Figure 16: Axial stress, σ_{yy} and transverse shear stress, σ_{yz} along the thickness of the composite sandwich-box beam.

stress allocations between 6×8L16 and 3D FEM models, which provide almost the same results.

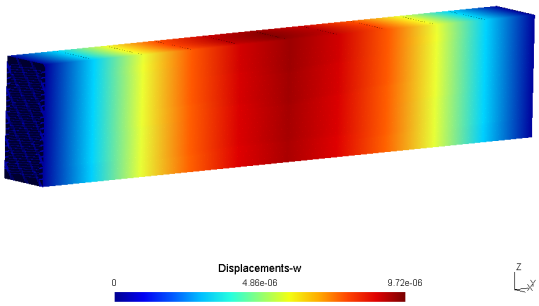

(a) 6×8L16, u_z

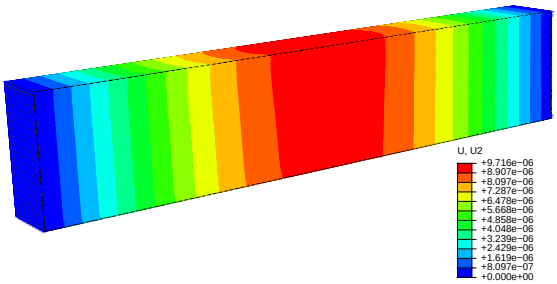

(b) ABAQUS, u_z

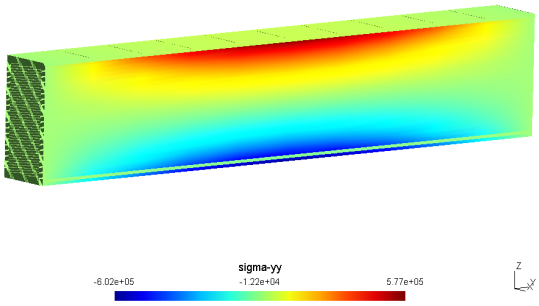

(c) 6×8L16, σ_{yy}

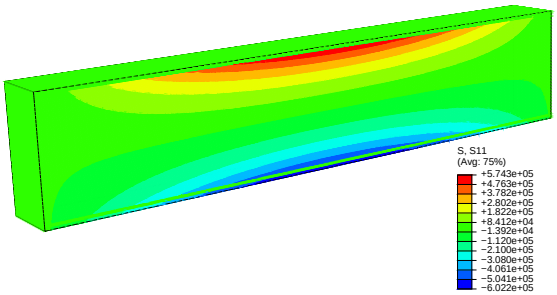

(d) ABAQUS, σ_{yy}

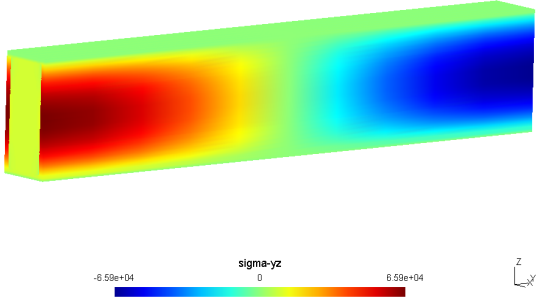

(e) 6×8L16, σ_{yz}

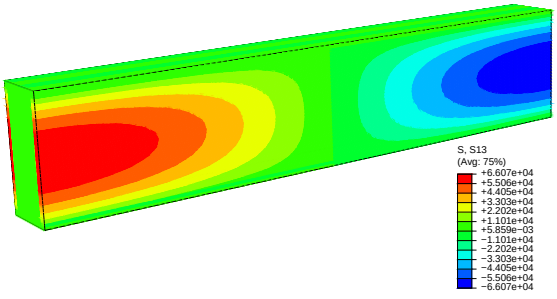

(f) ABAQUS, σ_{yz}

Figure 17: Comparison of the transverse displacement, u_z, the axial stress, σ_{yy} and transverse shear stress, σ_{yz}, by 6×8L16 and 3D FEM models.

7 Conclusions

In this paper, exact static analyses of cross-ply laminated and sandwich beams subjected to the simply supported boundary conditions and the transverse sinusoidal loading have been carried out by utilizing the refined beam model based on Lagrange Expansion within the framework of Carrera Unified Formulation. The CUF LE model expresses the 3D displacement field as the approximation of the arbitrary order of the displacement unknowns over the cross section. In this manner, higher-order Layer-Wise models can be formulated with ease. The principle of virtual work together with CUF LE has been subsequently used to formulate the strong-form governing equation, which can be solved via a Navier-type, close-form solution. The performance of the proposed model has been assessed by studying composite and sandwich beams with the geometrical shape of the cross section ranging from simple to complex and the obtained results are compared with those of available from previous studies and 3D FEM results computed by commercial code. The numerical results have shown that the proposed model can provide both displacements and stresses results with lower computational cost. Moreover, the correct detection of displacements and stresses distributions over the cross section is enabled. This capability is still valid when applied to composite structures with more complex structures, i.e., thin-walled composite box beam and composite sandwich-box beam. Furthermore, it should be underlined that, although sine loadings have been systematically considered, any kind of loading conditions can be studied with the present approach as they can be expressed as a Fourier expansion series [44].

Acknowledgments

E. Carrera has been partially supported by the Russian Science Foundation (Grant No. 15-19-30002).
Y. Yan acknowledges the support by the scholarship from the China Scholarship Council (CSC) (Grant No. 201606710014) and Fundamental Research Funds for the Central Universities (Grant No. 2014B31414).

References

[1] L. W. Zhang, M. F. Kai, and K. M. Liew. Evaluation of microstructure and mechanical performance of cnt-reinforced cementitious composites at elevated temperatures. *Composites Part A: Applied Science and Manufacturing*, 95:286–293, 2017.

[2] Y. Yan, Q. W. Ren, N. Xia, and L. F. Zhang. A close-form solution applied to the free vibration of the euler–bernoulli beam with edge cracks. *Archive of Applied Mechanics*, 86(9):1633–1646, 2016.

[3] T. Kant and B. S. Manjunath. Refined theories for composite and sandwich beams with c^0 finite elements. *Computers & structures*, 33(3):755–764, 1989.

[4] A. M. Zenkour. Transverse shear and normal deformation theory for bending analysis of laminated and sandwich elastic beams. *Mechanics of Composite Materials and Structures*, 6(3):267–283, 1999.

[5] J. N. Reddy. A simple higher-order theory for laminated composite plates. *Journal of Applied Mechanics*, 51(4):745–752, 1984.

[6] A. A. Khdeir and J. N. Reddy. Free vibration of cross-ply laminated beams with arbitrary boundary conditions. *International Journal of Engineering Science*, 32(12):1971–1980, 1994.

[7] D. K. Maiti and P. K. Sinha. Bending and free vibration analysis of shear deformable laminated composite beams by finite element method. *Composite Structures*, 29(4):421–431, 1994.

[8] M. Aydogdu. A new shear deformation theory for laminated composite plates. *Composite Structures*, 89(1):94–101, 2009.

[9] M. Karama, K. S. Afaq, and S. Mistou. Mechanical behaviour of laminated composite beam by the new multi-layered laminated composite structures model with transverse shear stress continuity. *International Journal of Solids and Structures*, 40(6):1525–1546, 2003.

[10] S. Mistou, M. Karama, B. Lorrain, and J. P. Faye. Analysis of sandwich composite beams with a new transverse shear stress continuity model. *Journal of Sandwich Structures and Materials*, 1(2):96–110, 1999.

[11] A. S. Sayyad and Y. M. Ghugal. Static flexure of soft core sandwich beams using trigonometric shear deformation theory. *Mechanics of Advanced Composite Structures*, 2(1):45–53, 2015.

[12] T. P. Vo and H. T. Thai. Static behavior of composite beams using various refined shear deformation theories. *Composite Structures*, 94(8):2513–2522, 2012.

[13] M. Lezgy-Nazargah, P. Vidal, and O. Polit. Nurbs-based isogeometric analysis of laminated composite beams using refined sinus model. *European Journal of Mechanics-A/Solids*, 53:34–47, 2015.

[14] J. N. Reddy. *Mechanics of laminated composite plates and shells: theory and analysis*. CRC press, 2004.

[15] N. J. Pagano. Exact solutions for composite laminates in cylindrical bending. *Journal of Composite Materials*, 3(3):398–411, 1969.

[16] J. F. Davalos, Y. Kim, and E. J. Barbero. Analysis of laminated beams with a layer-wise constant shear theory. *Composite Structures*, 28(3):241–253, 1994.

[17] R. P. Shimpi and Y. M. Ghugal. A new layerwise trigonometric shear deformation theory for two-layered cross-ply beams. *Composites Science and Technology*, 61(9):1271–1283, 2001.

[18] H. Arya, R. P. Shimpi, and N. K. Naik. Layer-by-layer analysis of a simply supported thick flexible sandwich beam. *AIAA journal*, 40(10):2133–2136, 2002.

[19] M. Tahani. Analysis of laminated composite beams using layerwise displacement theories. *Composite Structures*, 79(4):535–547, 2007.

[20] E. Carrera. Theories and finite elements for multilayered, anisotropic, composite plates and shells. *Archives of Computational Methods in Engineering*, 9(2):87–140, 2002.

[21] E. Carrera. Theories and finite elements for multilayered plates and shells: a unified compact formulation with numerical assessment and benchmarking. *Archives of Computational Methods in Engineering*, 10(3):215–296, 2003.

[22] E. Carrera and S. Brischetto. Analysis of thickness locking in classical, refined and mixed theories for layered shells. *Composite Structures*, 85(1):83–90, 2008.

[23] E. Carrera, G. Giunta, P. Nali, and M. Petrolo. Refined beam elements with arbitrary cross-section geometries. *Computers & Structures*, 88(5):283–293, 2010.

[24] A. Catapano, G. Giunta, S. Belouettar, and E. Carrera. Static analysis of laminated beams via a unified formulation. *Composite Structures*, 94(1):75–83, 2011.

[25] G. Giunta, S. Belouettar, H. Nasser, E. H. Kiefer-Kamal, and T. Thielen. Hierarchical models for the static analysis of three-dimensional sandwich beam structures. *Composite Structures*, 133:1284–1301, 2015.

[26] A. Pagani, E. Carrera, M. Boscolo, and J. R. Banerjee. Refined dynamic stiffness elements applied to free vibration analysis of generally laminated composite beams with arbitrary boundary conditions. *Composite Structures*, 110:305–316, 2014.

[27] B. Liu, L. Zhao, A. J. M. Ferreira, Y. F. Xing, A. M. A. Neves, and J. Wang. Analysis of viscoelastic sandwich laminates using a unified formulation and a differential quadrature hierarchical finite element method. *Composites Part B: Engineering*, 110:185–192, 2017.

[28] Y. Hui, G. Giunta, S. Belouettar, Q. Huang, H. Hu, and E. Carrera. A free vibration analysis of three-dimensional sandwich beams using hierarchical one-dimensional finite elements. *Composites Part B: Engineering*, 110:7–19, 2017.

[29] E. Carrera, A. Pagani, and J. R. Banerjee. Linearized buckling analysis of isotropic and composite beam-columns by carrera unified formulation and dynamic stiffness method. *Mechanics of Advanced Materials and Structures*, 23(9):1092–1103, 2016.

[30] G. Giunta, N. Metla, Y. Koutsawa, and S. Belouettar. Free vibration and stability analysis of three-dimensional sandwich beams via hierarchical models. *Composites Part B: Engineering*, 47:326–338, 2013.

[31] E. Carrera and M. Petrolo. Refined beam elements with only displacement variables and plate/shell capabilities. *Meccanica*, 47(3):537–556, 2012.

[32] E. Carrera, M. Filippi, P. K. R. Mahato, and A. Pagani. Advanced models for free vibration analysis of laminated beams with compact and thin-walled open/closed sections. *Journal of Composite Materials*, 49(17):2085–2101, 2015.

[33] E. Carrera, M. Filippi, P. K. R. Mahato, and A. Pagani. Accurate static response of single-and multi-cell laminated box beams. *Composite Structures*, 136:372–383, 2016.

[34] E. Carrera, M. Filippi, P. K. Mahato, and A. Pagani. Free-vibration tailoring of single-and multi-bay laminated box structures by refined beam theories. *Thin-Walled Structures*, 109:40–49, 2016.

[35] M. Filippi, A. Pagani, M. Petrolo, G. Colonna, and E. Carrera. Static and free vibration analysis of laminated beams by refined theory based on chebyshev polynomials. *Composite Structures*, 132:1248–1259, 2015.

[36] A. Pagani, A. G. De Miguel, M. Petrolo, and E. Carrera. Analysis of laminated beams via unified formulation and legendre polynomial expansions. *Composite Structures*, 156:78–92, 2016.

[37] A. Apuzzo, R. Barretta, M. Canadija, L. Feo, R. Luciano, and F. Marotti de Sciarra. A closed-form model for torsion of nanobeams with an enhanced nonlocal formulation. *Composites Part B: Engineering*, 108:315–324, 2017.

[38] R. Barretta, L. Feo, R. Luciano, F. Marotti de Sciarra, and R. Penna. Functionally graded timoshenko nanobeams: A novel nonlocal gradient formulation. *Composites Part B: Engineering*, 100:208–219, 2016.

[39] A. Apuzzo, R. Barretta, and R. Luciano. Some analytical solutions of functionally graded kirchhoff plates. *Composites Part B: Engineering*, 68:266–269, 2015.

[40] M. Dan, A. Pagani, and E. Carrera. Free vibration analysis of simply supported beams with solid and thin-walled cross-sections using higher-order theories based on displacement variables. *Thin-Walled Structures*, 98:478–495, 2016.

[41] Y. Yang, A. Pagani, and E. Carrera. Exact solutions for free vibration analysis of laminated, box and sandwich beams by refined layer-wise theory. *Composite Structures*, 175:28–45, 2017.

[42] E. Carrera, G. Giunta, and M. Petrolo. *Beam structures: classical and advanced theories*. John Wiley & Sons, 2011.

[43] E. Carrera, M. Cinefra, M. Petrolo, and E. Zappino. *Finite element analysis of structures through unified formulation*. John Wiley & Sons, 2014.

[44] G. Giunta, F. Biscani, S. Belouettar, and E. Carrera. Analysis of thin-walled beams via a one-dimensional unified formulation through a navier-type solution. *International Journal of Applied Mechanics*, 3(3):407–434, 2011.